# An Angle-Multiplexed Multifocal Method for D-Band 2D Beam-Scanning Transmitarray Leveraging 3D Transmission Line Component

Jiexin Lai, *Student Member, IEEE*, Xiaojing Lv, *Member, IEEE,* Md Mirazur Rahman, *Member, IEEE,* Md Ashif Islam Oni, *Member, IEEE,* Shuvashis Dey, *Member, IEEE* and Yang Yang, *Senior Member, IEEE*

***Abstract*—This paper proposes an angle-multiplexed multifocal method for designing a 2D beam-scanning transmitarray (TA). The angle-multiplexed method is commonly used to generate orbital angular momentum (OAM) multiplexing. The multifocal phase distribution (PD) is calculated using the combination of the angle-multiplexed and bifocal methods to achieve higher gain enhancement and 2D beam-scanning with a low scan loss without optimisation. The additive manufacturing technology is used to fabricate a 3D transmission line component. In the terahertz band, the transmitting and receiving (Tx-Rx) unit cell (UC) impedance matching can be affected by the Pancharatnam-Berry (P-B) method, and a 3D coaxial line is introduced to tackle this problem. For proof of concept, the prototype was fabricated. Feeded by a WR-06 waveguide probe, the proposed TA achieves a gain enhancement of 16.3 dB and ±30° 2D beam-scanning, simulated and measured 3-dB gain bandwidths of 19.6% and 16.3%, and the measured axial ratio (AR) bandwidth of 30.7%.**

***Index Terms*—Circular polarisation, transmitarray (TA), terahertz (THz), D-band, additive manufacturing, multifocal.**

## I. INTRODUCTION

TERAHERTZ (THz) spectrum (0.1-10 THz) is getting increasing attention. Recently, the THz frequency band from 95 GHz to 3 THz has been announced for sixth-generation (6G) mobile communication experiments, which will integrate the connection between air, space and ground [1]. THz waves can offer broadband communication for inter-satellites, and there is little atmospheric absorption in the vacuum environment. Transmitarrays (TAs) can realise a high gain, high directivity and beam-scanning performance, and circularly polarised (CP) antennas mitigate polarisation mismatch in space. Thus, THz CP beam-scanning TAs are potentially vital for future intersatellite 6G communication.

Beam-scanning TAs can be classified into three categories: TAs with a focal plane [2], [3], a focal arc [4] and a focal locus [5]. TAs with a planar feed source antenna array have attracted much attention because they suit planar high-precision and economical PCB fabrication techniques. Therefore, the TA with a focal plane is more desirable. To achieve a multibeam TA, the multibeam phase distribution (PD) must compensate several PDs with different incident angles, minimising their phase errors. Thus, unifocal [3], bifocal [6]-[8] and multifocal [4], [9], [10] methods have been proposed. The bifocal method relies on averaging PDs of two single focal PDs, and optimisation algorithms are partly needed, while the multifocal method almost definitely requires optimisation algorithms.

As the operating frequency rises, the minimum design feature for the TA is nearing the limits of printed circuit board (PCB) technology accuracy, posing challenges for the design of THz unit cells (UCs). Designing THz TA UCs with simple structures is anticipated to mitigate fabrication challenges. According to open literature, THz TA UCs can be realised using 3D printed dielectric post [11], [12], the Fabry-Perot-like resonator [13], [14], frequency-selective surface (FSS) [15], [16], Huygens UC [17], and transmitting and receiving (Tx-Rx) UCs [18], [19]. However, only a few papers have proposed THz TA for converting linear polarisation to circular polarisation (LP-CP). In [20], 3D printing has been applied to design CP THz TAs, using dielectric UCs incorporating CP polarisers to achieve LP to CP conversion. In lower frequencies, the LP-CP Tx-Rx UCs include a U-shaped slot [21], [22], the off-centre feeding point [23], [24], and the CP antenna [25]-[27]. Statistically, the gap between the ground hole and the metal via is about $0.01\lambda_0$ (central wavelength $\lambda_0$) in these papers, which reaches the limits of standard PCB fabrication in the THz band.

This work presents a Sub-THz wideband LP-CP TA for ±30° 2D beam-scanning applications. A new angle-multiplexed multifocal PD calculation method is proposed for 2D beam-steering with a higher gain enhancement without additional optimisation. A coaxial-line-based UC is proposed for a better Pancharatnam-Berry (P-B) phase performance. The first D-band conductive and dielectric multimaterial LP-CP TA was achieved using additive manufacturing, reaching the highest achievable frequency range within the precision limits of additive manufacturing. The proposed 26×26 LP-CP TA realised a high gain enhancement of 16.3 dB compared with the standard waveguide probe of WR-06. The simulated and measured 3-dB gain bandwidths are 19.6% and 16.3%.

Manuscript received XX;. This work was supported in part by the Australian Research Council (ARC) Linkage Infrastructure Equipment and Facilities underGrant LE220100035, in part by the Linkage Project under Grant LP210300004, and in part by the New South Wales Space Research Network Pilot Project. (Corresponding author: Yang Yang.)

Jiexin Lai, Xiaojing Lv and Yang Yang are with school of Electrical and Data Engineering, University of Technology Sydney, Ultimo, NSW 2007, Australia.

Shuvashis Dey, Md Mirazur Rahman and Md Ashif Islam Oni are with Department of Electrical and Computer Engineering, North Dakota State University, Fargo, ND-58102, United States.

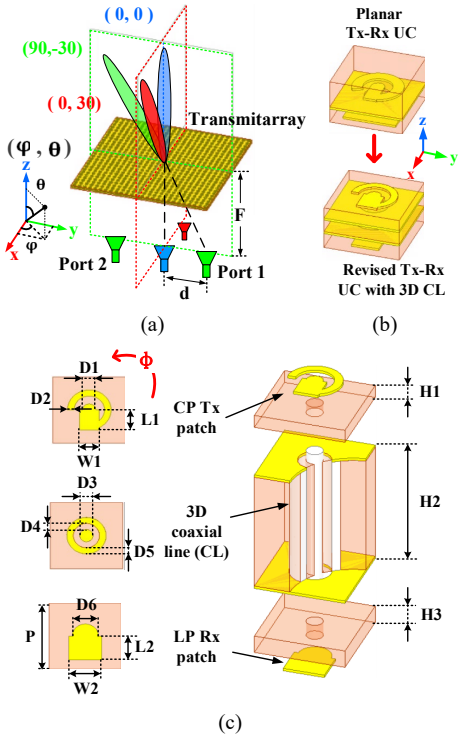


Fig. 1. (a) Coordinate system of the proposed TAA with three feed sources. (b) Structure of the planar and revised UC (c) Exploded diagrams and details: H1 = 0.175, H2 = 0.2, H3 = 0.24, L1 = 0.33, L2 = 0.4, W1 = 0.3, W2 = 0.5, D1 = 0.2, D2 = 0.1, D3 = 0.2, D4 = 0.1, D5 = 0.1, D6 = 0.4, P = 1.1. Units: mm. Φ is the rotation angle of the CP Tx patch.

## II. Unit Cell Design

The proposed designs are fabricated using an additive manufacturing technique [28]-[31]. The arbitrary thickness of the dielectric layer ($\varepsilon_r = 2.7$, tanδ = 0.04 at D-band) can be obtained. The accuracy reached through this method is approximately 36 μm for printing the conductive layer. The accuracy of the thickness of the dielectric layer is about 17 $\mu m$. The minimum width of the conductive layer is 100 $\mu m$, and the minimum diameter of the metallic via is 200 $\mu m$. The coordinate system of the proposed TAA with several feed sources and three beams is shown in Fig. 1 (a). In Fig. 1 (b), a planar Tx-Rx UC utilizes a ground hole and a metal via as a connection between the LP Rx patch and the CP Tx patch for the right-hand circularly polarised (RHCP) wave generation. A three-dimensional coaxial line (CL) is introduced in the revised UC, and the size of the patches is optimised for impedance matching in the same frequency band. Fig.1 (c) shows an exaggerated structure; the actual size depends on the data. The coaxial line and the patches are made of the same material, and the different colours are only used to distinguish them. As shown in Fig. 2, rotating the CP patch of the planar UC without the coaxial line will significantly impact the reflection and transmission coefficients. Because the gap between the ground hole and metal via is 0.1 mm ($0.04\lambda_0$ @ 125 GHz) and can not be reduced due to the manufacturing precision.

The simulated performance of the revised UC with the coaxial line is given in Fig. 3. A wide -10 dB bandwidth is from 116.7 GHz to 142.4 GHz (19.8%) for any rotation angles. The peak transmission coefficient from X to RHCP polarised waves is -2 dB, which includes a 1.5 dB loss introduced by the lossy substrate, and the normalised -1 dB bandwidth is from 116 GHz to 141.1 GHz (19.5%). The UC can provide a 360° phase modulation.

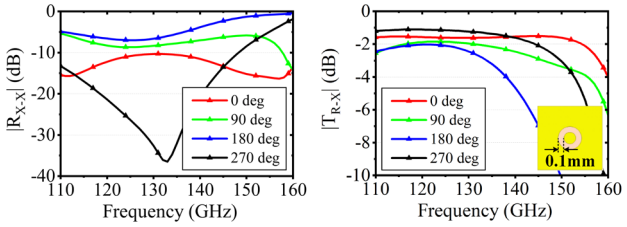


Fig. 2. P-B performance of the planar UC without the coaxial line. (a) Reflection coefficients and (b) transmission coefficients. $|R_{X-X}|$ represents the reflection coefficient from X to X polarised waves. $|T_{R-X}|$ represents the transmission coefficient from X to RHCP waves.

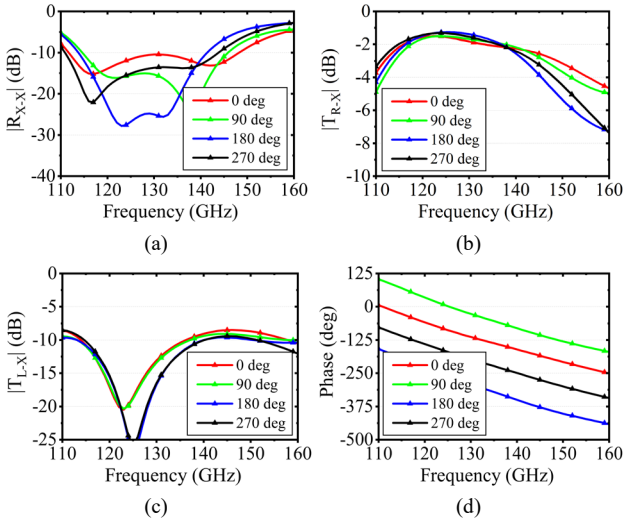


Fig. 3. P-B performance of the revised UC with the coaxial line. (a) Reflection coefficients from X to X polarised waves; (b) transmission coefficients from X to RHCP waves; (c) Transmission coefficients from X to LHCP waves, (d) Transmission phase of $|T_{R-X}|$.

## III. Angle-Multiplexed Multifocal Method

### A. 1D Bifocal PD Calculation

The proposed CP UC is designed for a 26×26 TA. A TA with a focal plane is designed for beam-scanning applications. For comparison, the bifocal method [6]-[8] and the angle-multiplexed multifocal method are adopted to calculate the PD for 1D beam-scanning. The related coordinate system is depicted in Fig. 1 (a), $\theta$ is the titled angle of the radiation beam, $d$ represents the offset of port 1 to the centre. The common bifocal PDs for port 1 and port 2 can be given by:

$$\Psi_1 = k_0(\sqrt{x^2 + (y-d)^2 + F^2} + y * sin\theta) \quad (1)$$

$$\Psi_2 = k_0(\sqrt{x^2 + (y+d)^2 + F^2} - y * sin\theta) \quad (2)$$

$$\Psi_{bifocal\_1} = (\Psi_1 + \Psi_2)/2 \quad (3)$$

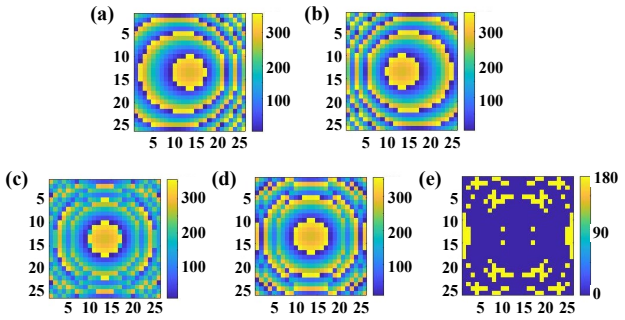


Fig. 4. Phase distributions (PDs) at 125 GHz. (a) (b) PD $\Psi_1$, $\Psi_2$ fed by port 1 and 2 only for a single tilted beam, as shown in the coordinate system in Fig. 1 (a). (c) Common bifocal PD, $\Psi_{bifocal\_1}$. (d) Angle-multiplexed bifocal PD, $\Psi_{bifocal\_2}$. (e) The difference between $\Psi_{bifocal\_1}$ and $\Psi_{bifocal\_2}$.

where $k_0$ is the wave number in free space, and $(x, y)$ is the position of the transmitarray unit cell. The focal length is 12 mm, and the θ is set to 30°. Two single-focal PDs $\Psi_1$ and $\Psi_2$ are shown in Fig. 4 (a) and (b), respectively. The common bifocal PD is presented in Fig. 4 (c). The basic principle of the bifocal method is based on similar PDs for two focal points. When the following equation holds:

$$d = F * tan\theta \tag{4}$$

The centres of the two single-focal PDs are located in the centre of the transmitarray, which can minimise the phase errors of the $\Psi_{bifocal\_1}$. On the other hand, the authors take an initial approach by adopting the angle-multiplexing technique adapted from OAM metasurface designs [32], [33].

$$\Psi_{bifocal\_2} = angle[exp(j\Psi_1) + \exp(j\Psi_2)] \tag{5}$$

$angle[\cdot]$ is used to obtain the complex phase angle. The angle-multiplexed PD is shown in Fig. 4 (d). The difference between both in Fig. 4 (e) has two numbers, 0 and 180 deg, meaning $\Psi_{bifocal\_1}$ and $\Psi_{bifocal\_2}$ have an almost similar pattern. The angle-multiplexed multifocal method was first validated in a 1D application scenario, demonstrating that it can achieve equally accurate results without adding complexity to the computational algorithm. The advantages of this approach become significantly more evident in the following subsection for 2D application scenario.

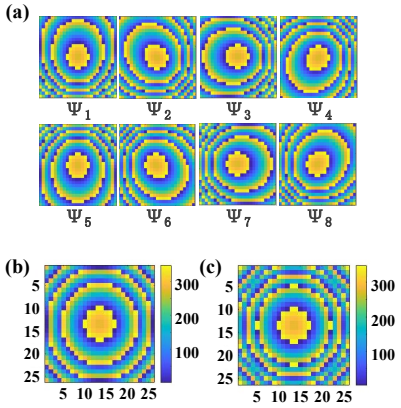


Fig. 5. Phase distributions (PDs) at 125 GHz. (a) Eight PDs for a single tilted beam. (b) Conventional bifocal PD, $\Psi_{multi-focal\_1}$. (c) Angle-multiplexed PD, $\Psi_{multi-focal\_2}$

## B. 2D Multifocal TA Design

When designing for a 2D beam-scanning TA, the difference between the common and angle-multiplexed method increases. Fig. 5 (a) shows eight PDs for a single tilted beam, and Fig. 5 (b) and (c) are the combination of these PDs using the common and angle-multiplex methods. These PDs can be calculated by:

$$\Psi_n = k_0(\sqrt{(x - d * cos\varphi_n)^2 + (y - d * sin\varphi_n)^2 + F^2} - sin\theta * [x * \cos(\varphi_n + \pi) + y * \sin(\varphi_n + \pi)]) \tag{6}$$

$$\varphi_n = (n-1)\frac{\pi}{4} \quad n=1, 2, 3, \dots, 8$$

$$\Psi_{multi-focal\_1} = \frac{1}{8}\sum_{n=1}^{8}\Psi_n \tag{7}$$

$$\Psi_{multi-focal\_2} = angle[\sum_{n=1}^{8} exp(j\Psi_n)] \tag{8}$$

where the parameter $\varphi_n$ represents the angle between the focal point and the X-axis. The $\varphi_n + \pi$ is the direction of the TA radiation beam. The simulated radiation patterns and gains versus frequency are shown in Fig. 6. The simulated results are based on a lossless material to show the improvement of the proposed method. The beams for the direction of $(\varphi, \theta)$ have been coloured: red for the plane of $\varphi = 0°$, and green for the plane of $\varphi = 90°$. The plane of $\varphi = 45°$ (black) is omitted for clarity. They are correlated with the radiation

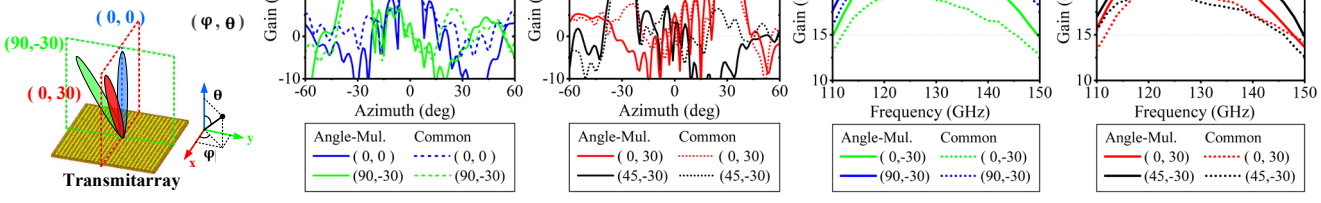


Fig. 6. Comparison between the angle-multiplexed and common method with a lossless material. (a) Schematic of three beams. (b) and (c) Radiation patterns at 125 GHz. (d) and (e) Gain versus frequency of four beams.

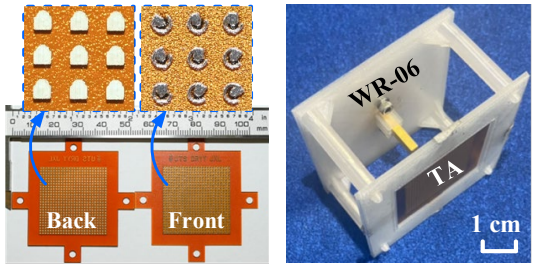


(a) (b)

Fig. 7. (a) Back and front of the prototype and the zoom-in image. (b) Transmitarray antenna.

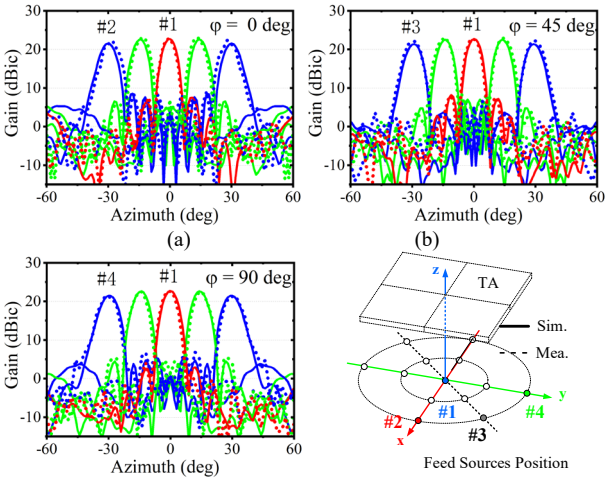


Fig. 8. Measured and simulated radiation patterns at 125 GHz in the plane of (a) $\varphi = 0°$, (b) $\varphi = 45°$, and (c) $\varphi = 90°$. (d) The position of four feed sources with marks under the TA. Solid line: simulated results. Dash line: measured results.

patterns beside. In Fig. 6 (b) and (c), the gains of four beams by using the common method are 21.6 dBic for the direction of $(\varphi = 0°, \theta = 0°)$, 19.8 dBic for $(\varphi = 0°, \theta = 30°)$, 19.1 dBic for $(\varphi = 90°, \theta = -30°)$, and 19.2 dBic for $(\varphi = 45°, \theta = -30°)$. By comparison, the gains by using the angle-multiplexed method are 24.8 dBic, 23.6 dBic, 23.8 dBic and 23.6 dBic. In Fig. 6 (d) and (e), compared with the common method, about 3-4 dB gain enhancement and 1.2 dB scan loss are achieved by using the angle-multiplexed method.

## IV. Result and Discussion

The prototype is shown in Fig. 7. The TA is fed by the standard WR-06 waveguide probe. The measured and simulated radiation patterns at 125 GHz are presented in Fig. 8. The beams' directions are $-30°$, $-15°$, $0°$, $15°$, and $30°$.

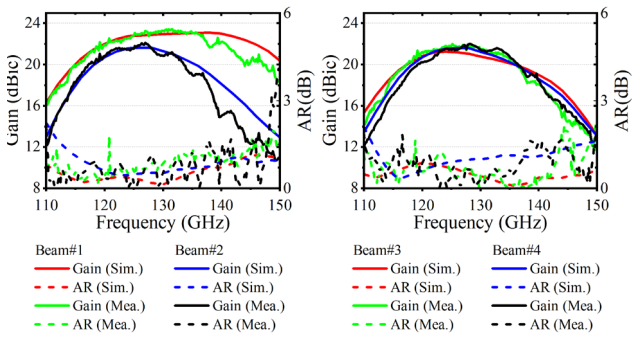


(a) (b)

Fig. 9. Measured and simulated gain and AR. (a) Beam #1 and Beam #2. (b) Beam #3 and Beam #4.

Seven beams have been marked from #1 to #7, and their related feed sources position is plotted in Fig. 8 (d); the related position of the seven points are (0,0), (3.5,0), (7,0), (2.47,2.47), (4.95,4.95), (0,3.5), and (0,7). The simulated gain of the TA reduces to 22.7 dBic with a scan loss of 1.2 dB, while the measured one is 19.6 dBic and 0.7 dB.

The simulated and measured gain and AR curves versus frequency for various beams are shown in Fig 9. The simulated overlapped 3-dB gain bandwidth for beams #1-#7 is from 114 GHz to 138 GHz (19.6%), and the AR bandwidth is from 110 GHz to 145 GHz (27.4%). The measured overlapped 1-dB and 3-dB gain bandwidth and the AR bandwidth are from 120.6 to 133.8 GHz (10.4%), from 116.2 to 136.8 GHz (16.3%) and 110 to 150 GHz (30.7%) for various beams. The average beam scan loss is about 1.7 dB. The performance comparison is given in Table I. The increase in feed source gain can lead to an increase in TA antenna gain. Therefore, the gain enhancement compared to the feed source is discussed to show the performance of the TA only. The proposed TA can achieve a higher gain enhancement of 16.3 dB using the angle-multiplexed multifocal method, even including a 2-3 dB material loss. The gain increase is partly at the cost of the gain bandwidth and beam coverage.

## V. Conclusion

The proposed sub-THz CP TA for 2D beam-scanning can realise a high gain enhancement of 16.3 dB, the polarisation conversion from LP to CP, and a wide 2D beam-scanning range of $\pm 30°$ with a scan loss of 1.7 dB. The angle-multiplexed multifocal method is superior for 2D beam-scanning to achieve a higher gain. The proposed TA is a promising candidate for future inter-satellite communication.

TABLE I
Performance Comparison with Other Transmitarrays

| Ref. | Freq (GHz) | Pol. | F/D | Gain (dBi) | Gain Enhancement (dB) | 1dB Gain BW | 3dB Gain BW | AR BW | Beam Coverage | Scan Loss (dB) | Thickness ($\lambda_0$) |
|---|---|---|---|---|---|---|---|---|---|---|---|
| [2] | 27 | LP-CP | 0.44 | 21.5 | 11.5 | N.G. | 33.3% | 40.7% | ±33° (1D) | 2 | 0.39 |
| [8] | 26 | CP | 0.37 | 21.4 | 13.4 | N.G. | 20.0% | 20.0% | ±33° (2D) | 1.2 | 0.27 |
| [17] | 200 | LP | 2.47 | 29 | 7 | N.G. | 19.1% | N.A. | ±48° (1D) | 2.85 | 0.17 |
| [20] | 300 | LP-CP | 2 | 30 | 7 | 13.3% | 13.3% | 18.8% | N.A. | N.A. | 2.40 |
| Proposed | 125 | LP-CP | 0.42 | 22.8 | 16.3 | 10.4% | 16.3% | 30.7% | ±30° (2D) | 1.7 | 0.28 |

N.G. : Not Given; N.A. : Not Applicable

## REFERENCES

[1] B. Ji; Y. Han; S. Liu; F. Tao; G. Zhang; Z. Fu., "Several key technologies for 6G: challenges and opportunities," in *IEEE Communications Standards Magazine*, vol. 5, no. 2, pp. 44-51, June 2021.

[2] Z. H. Jiang, Y. Zhang, J. Xu, Y. Yu and W. Hong, "Integrated broadband circularly polarised multi-beam antennas using Berry-phase transmit-arrays for Ka-band applications," in *IEEE Transactions on Antennas and Propagation*, vol. 68, no. 2, pp. 859-872, Feb. 2020.

[3] P. Mei, G. F. Pedersen and S. Zhang, "Performance improvement of mechanically beam-steerable transmitarray antennas by using offset unifocal phase symmetry," in *IEEE Transactions on Antennas and Propagation*, vol. 71, no. 1, pp. 1129-1134, Jan. 2023

[4] P. Nayeri, F. Yang and A. Z. Elsherbeni, "Design of multifocal transmitarray antennas for beamforming applications," in *2013 IEEE Antennas and Propagation Society International Symposium (APSURSI)*, Orlando, FL, USA, 2013, pp. 1672-1673.

[5] L. -Z. Song, M. Ansari, P. -Y. Qin, S. Maci, J. Du and Y. J. Guo, "Two-dimensional wide-angle multibeam flat grin lens with a high aperture efficiency," in *IEEE Transactions on Antennas and Propagation*, vol. 71, no. 10, pp. 8018-8029, Oct. 2023

[6] P. Nayeri, F. Yang and A. Z. Elsherbeni, "Bifocal design and aperture phase optimisations of reflectarray antennas for wide-angle beam scanning performance," in *IEEE Transactions on Antennas and Propagation*, vol. 61, no. 9, pp. 4588-4597, Sept. 2013.

[7] X. Tong; Z. H. Jiang; H. Chen; F. Wu; J. Cao; R. Sauleau, "A dual-CP multibeam transmit-array antenna based on anisotropic impedance surfaces and hybrid phase compensation," in *IEEE Antennas and Wireless Propagation Letters*, vol. 22, no. 5, pp. 1144-1148, May 2023

[8] J. Hu, H. Wong and L. Ge, "A circularly-polarized multi-beam magneto-electric dipole transmitarray with linearly-polarised feeds for millimeter-wave applications," in *IEEE Transactions on Antennas and Propagation*, vol. 70, no. 7, pp. 6012-6017, July 2022.

[9] G. -B. Wu, S. -W. Qu and S. Yang, "Wide-angle beam-scanning reflectarray with mechanical steering," in *IEEE Transactions on Antennas and Propagation*, vol. 66, no. 1, pp. 172-181, Jan. 2018.

[10] Á. F. Vaquero, J. Teixeira, S. A. Matos, M. Arrebola; J. R. Costa, J. M. Felício, "Design of low-profile transmitarray antennas with wide mechanical beam steering at millimeter waves," in *IEEE Transactions on Antennas and Propagation*, vol. 71, no. 4, pp. 3713-3718, April 2023.

[11] Wu G B, Chan K F, Chan C H. 3-D printed terahertz lens to generate higher order Bessel beams carrying OAM. in *IEEE Transactions on Antennas and Propagation*, 2020, 69(6): 3399-3408.

[12] J. Lai, X. Lv and Y. Yang, "A 3-D printed 140 GHz multifocal dielectric transmitarray antenna for 2-D mechanical beam scanning," in *IEEE Antennas and Wireless Propagation Letters*, vol. 23, no. 4, pp. 1366-1370, April 2024.

[13] L. Song, T. Zhang, P. -Y. Qin, J. Du and Y. J. Guo, "Sub-THz broadband transmitting metasurfaces with enhanced frequency-scanning capability," in *IEEE Transactions on Terahertz Science and Technology*, vol. 14, no. 1, pp. 82-90, Jan. 2024.

[14] O. Koutsos, F. F. Manzillo, M. Caillet, R. Sauleau and A. Clemente, "Experimental demonstration of a 43-dBi gain transmitarray in PCB technology for backhauling in the 300-GHz band," in *IEEE Transactions on Terahertz Science and Technology*, vol. 13, no. 5, pp. 485-492, Sept. 2023

[15] W. Saleh, Y. Letestu, R. Sauleau and E. M. Cruz, "Design and measurements of a high-performance wideband transmitarray antenna for D-band communications," in *IEEE Antennas and Wireless Propagation Letters*, vol. 20, no. 9, pp. 1765-1769, Sept. 2021.

[16] D. Seo, H. Kim, S. Oh, J. Kim and J. Oh, "Ultrathin high-gain D-band transmitarray based on a spatial filter topology utilizing bonding layer effect," in *IEEE Antennas and Wireless Propagation Letters*, vol. 21, no. 10, pp. 1945-1949, Oct. 2022

[17] L. -Z. Song, T. Zhang, J. -X. Lai, Y. Yang and J. Du, "A 180-GHz to 220-GHz wideband transmitarray with wide-angle beam steering for intersatellite communications," in *IEEE Transactions on Antennas and Propagation*, vol. 72, no. 1, pp. 950-955, Jan. 2024.

[18] Z. -W. Miao Z. -C. Hao; G. Q. Luo; L. Gao; J. Wang; X. Wang, "140 GHz high-gain LTCC-integrated transmit-array antenna using a wideband SIW aperture-coupling phase delay structure," in *IEEE Transactions on Antennas and Propagation*, vol. 66, no. 1, pp. 182-190, Jan. 2018.

[19] F. Foglia Manzillo, A. Clemente and J. L. González-Jiménez, "High-gain D-band transmitarrays in standard PCB technology for beyond-5G communications," in *IEEE Transactions on Antennas and Propagation*, vol. 68, no. 1, pp. 587-592, Jan. 2020.

[20] G. B. Wu, Y. -S. Zeng, K. F. Chan, S. -W. Qu and C. H. Chan, "High-gain circularly polarized lens antenna for terahertz applications," in *IEEE Antennas and Wireless Propagation Letters*, vol. 18, no. 5, pp. 921-925, May 2019.

[21] F. Diaby, A. Clemente, K. T. Pham, R. Sauleau and L. Dussopt, "Circularly polarized transmitarray antennas at Ka-band," in *IEEE Antennas and Wireless Propagation Letters*, vol. 17, no. 7, pp. 1204-1208, July 2018.

[22] J. Wang, X. Zhang, J. Ding, H. Zhang, W. Chen and C. Chen, "Characteristic mode inspired broadband circularly polarised folded transmitarray antenna," in *IEEE Transactions on Antennas and Propagation*, vol. 71, no. 9, pp. 7632-7637, Sept. 2023.

[23] H. Kaouach, "Design and characterisation of circularly polarized discrete lens antennas in 60-GHz band," in *IEEE Antennas and Wireless Propagation Letters*, vol. 15, pp. 1200-1203, 2016.

[24] C. Yang, G.-B. Wu, D. Zheng, K. F. Chan and C. H. Chan, "An ultralow-profile folded transmitarray antenna based on a multifunctional metasurface with both-sided wavefront control," in *IEEE Transactions on Antennas and Propagation*, vol. 71, no. 10, pp. 7804-7812, Oct. 2023.

[25] X. Dai, G. -B. Wu and K. -M. Luk, "A wideband circularly polarized transmitarray antenna for millimeter-wave applications," in *IEEE Transactions on Antennas and Propagation*, vol. 71, no. 2, pp. 1889-1894, Feb. 2023.

[26] L. Xiang, F. Wu, Z. -W. Miao, Z. H. Jiang, C. Yu and W. Hong, "A wideband circularly polarised magnetoelectric dipole transmitarray antenna based on element rotation techniques," in *IEEE Transactions on Antennas and Propagation*, vol. 71, no. 8, pp. 6953-6958, Aug. 2023.

[27] H. Lei, Y. Liu, Y. Jia, Y. Zhong and Z. -X. Liu, "A low-profile 2-D beam-scanning circularly polarized antenna combining reflectarray and transmitarray," in *IEEE Antennas and Wireless Propagation Letters*, EarlyAccess.

[28] J. Zhu, M. Li, J. Lai, Y. Yang, "Multimaterial additively manufactured transmissive spin-decoupled polarisation-maintaining metasurfaces," in *Laser & Photonics Reviews*, vol. 17, no. 12, pp. 2300433, Dec. 2023.

[29] J. Zhu, Y. Yang, F. Wang, J. Lai, "3D printed spin-decoupled transmissive metasurfaces based on versatile broadband cross-polarisation rotation meta-atom," in *Advanced Optical Materials*, vol. 11, no. 4, pp. 2202416, Feb. 2023.

[30] J. Zhu, Y. Yang, J. Lai, J. Nulman, "Additively manufactured polarisation insensitive broadband transmissive metasurfaces for arbitrary polarization conversion and wavefront shaping," in *Advanced Optical Materials*, vol. 10, no. 21, pp. 2200928, Nov. 2022.

[31] J. Zhu, Y. Yang, J. Lai, M. Li, "3-D printed noninterleaved reflective metasurfaces supporting dual-band spin-decoupled quadruplex channel independent beam-shaping with controllable energy distribution," in *IEEE Transactions on Microwave Theory and Techniques*, vol. 72, no. 2, pp. 1196-1205, Feb. 2024.

[32] L. Wang, Y. Yang, L. Deng, W. Hong, C. Zhang, S. Li, "Terahertz angle-multiplexed metasurface for multi-dimensional multiplexing of spatial and frequency domains," in Advanced Theory and Simulations, vol. 3, no. 10, pp. 2000115, Oct 2020.

[33] Y. Li, X. Li, L. Chen, M. Pu, J. Jin, M. Hong, X. Luo, "Orbital angular momentum multiplexing and demultiplexing by a single metasurface," in *Advanced Optical Materials*, vol. 5, no. 2, pp. 1600502, Jan 2017.